Dr. Kai Schröter and two anonymous referees
Natural Hazards and Earth System Sciences

Dear Dr. Schröter and Referees,

Please find enclosed our resubmission containing suggested revisions from two anonymous referees for our article entitled "Pre-disaster mapping with drones: an urban case study in Victoria, BC, Canada" by Maja Kucharczyk and Chris Hugenholtz.

We would like to thank the two anonymous referees for their constructive, helpful, and thorough reviews that have improved this paper. The referee comments mainly pertained to the transferability of the methodology to different urban areas, and the methods used in the vertical accuracy assessment. We believe that we have sufficiently addressed the comments and provided additional clarification where necessary.

A record of all changes to the manuscript can be found in the attached marked-up manuscript. Below, we address each referee comment. Each referee comment is in **BOLD** and our response directly below. Page/line numbers in referee comments refer to the original submission. Page/line numbers in responses refer to lines in the marked-up manuscript showing tracked changes.

Thank you for your continued consideration of our article for publication in *Natural Hazards and Earth System Sciences*.

Sincerely,

Maja Kucharczyk and Chris Hugenholtz

__**Comments from Anonymous Referee #1:**__

GENERAL COMMENTS

1. **The manuscript presents an interesting study about the potential of terrain elevation data sets and façade images generated from unmanned aerial vehicles (UAVs, also known as drones) to support post-disaster rescue decision making. The study has also a strong practical relevance.**

2. **In my opinion, a discussion on the applicability of the proposed data acquisition methods in different conditions from those in Victoria (Canada), e.g. different types of buildings or different city layouts, and also the limitations related to building destruction and weather conditions can impose on the fly-ability of UAVs, should be included in the manuscript.**
    - We thank the referee for this important consideration. We added the following paragraph to the end of Section 4.2: "The data acquisition methods used in this study will need to be adapted to fit the conditions of different urban areas. For example, flight altitude will need to be adjusted to give a safe vertical clearance from the tallest building. If the terrain in the area is sloped, elevation data should be input to the flight planning software to keep the flight altitude constant. A grid of flight lines is recommended, although its orientation and image overlap will vary depending on factors such as building layout and density. In a post-disaster context, a takeoff and landing location may be difficult to locate and access due to widespread destruction. Weather conditions such as high winds and rain following storm events may pose challenges to the flying ability of lightweight drones. Atmospheric conditions such as haze and smoke limit optical sensors in imaging destruction. These factors are examples of considerations that should be made when adapting the data acquisition methodology in this study".

3. **In general, the manuscript is well written and clear, and the figures and tables are informative and of good quality. Below I suggest a few minor points that the authors may consider to improve the quality of the manuscript**

SPECIFIC COMMENTS

4. **Page 1, Lines 14-15. This sentence should be rephrased/improved as it is too general and not completely correct, as it ignores many factors that may minimise the impact of natural hazards in cities (increased quality of construction, alarm systems, proximity to rescue services, . . .).**
    - We thank the referee for this important point. On page 1, lines 14-17, we revised the sentence and the proceeding sentence as such: "Increasing global population and urbanization (particularly in vulnerable areas) are factors that can contribute to increased death and destruction by natural hazards like earthquakes and tropical cyclones. In addition to initiatives such as increased quality of construction, alarm systems, and proximity to rescue services, pre-disaster mapping can help increase a city's resilience against disasters (Pu, 2017)".
5. **Page 3, Line 4: according to many guidelines the % symbol should not be preceded by a space. This happens in many other parts of the manuscript. Please consider to revise**
    - We followed the NHESS manuscript preparation guidelines (link below) when we decided to include spaces between numbers and units (e.g., %, m, °). The specific guideline is listed under the section "Manuscript composition", subsection "Figure

content guidelines", item 4: "Spaces must be included between number and unit (e.g. 1 %, 1 m)". The description for "Figure content guidelines" reads "In order to facilitate consistency with our language and typesetting guidelines applied to the text of the manuscript, please keep the following in mind when producing your figures". Therefore, we interpreted these figure guidelines to be applicable to the text. However, if our interpretation is incorrect, we will remove the spaces between numbers and the % symbol.

- NHESS manuscript preparation guidelines we consulted: https://www.natural-hazards-and-earth-system-sciences.net/for_authors/manuscript_preparation.html

6. **Page 3, Line 5: ". . . report. . . conducted. . .". I believe reports do not conduct assessments. Perhaps "present". Please consider to adjust the sentence.**
   - On page 3, line 6, we replaced "conducted" with "presented": "A 2016 report on the seismic vulnerability of Victoria ~~conducted~~ presented a risk assessment…".

7. **Page 5, Line 2: "GNSS" all acronyms should be defined when they are used for the 1st time in the text to avoid ambiguity. Is GNSS the acronym for "Global Navigation Satellite System"? Please check other acronyms that are not defined in the manuscript.**
   - Page 5, lines 10-11: we defined GNSS
   - We also defined SODA (page 4, line 17), RGB (page 4, line 17), NRCan (page 4, line 26), and CGG2013 (page 6, line 5).

8. **Page 6, Line 13: a reference to the software should be added.**
   - Page 7, line 18: We added an in-text citation to CloudCompare software. We added the citation to the reference list.
   - For consistency, we also added in-text citations for senseFly eMotion (page 4, line 28), Pix4D Pix4Dmapper (page 5, line 12), and ESRI ArcMap (page 7, line 9), and added them to the reference list.

9. **Page 6, Line 16: "to" seems to be missing in the sentence**
   - Page 6, line 14: We added "to" to the following: "ASPRS (2015) recommend vertical checkpoints to be…".

10. **Page 8, Line 1: a "that" seems to be missing in this sentence**
    - Page 8, line 18: We added "that" to the following: "With a 0.31 m average point spacing, it is possible that the LiDAR point cloud…".

11. **Page 8, Line 24: "was assessed going forward"? what do the authors mean with this? Please consider to rephrase the sentence.**
    - Page 9, lines 8-9: After considering this comment, we realized this sentence is unnecessary, and have removed it from the text.

12. **Page 9, Line 27: "single story building" instead?**
    - We would like to retain "single building story" because the use of DSMs to detect building collapse can include partial collapses such as single-story collapse (Fig. 1) and roof collapse (Fig. 2) within a multi-story building. We believe "single building story" is the more general term, as it includes single-story buildings and partial collapses.

Fig. 1. Single-story collapse. Copied from So (2016).

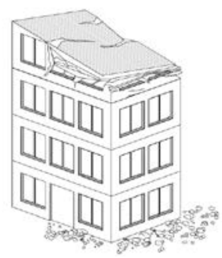

Fig. 2. Roof collapse. Copied from So (2016).

So, E. (2016). *Estimating Fatality Rates for Earthquake Loss Models.* London: Springer.

13. Page 9, Line 32: should read ". . . sub-meter LoDs. . ." instead of sub-decimeter?

- We thank the referee for identifying this error. On page 10, line 19, we changed "sub-decimeter" to "sub-meter".

14. Page 10, Line 25: ", . . . but achieve a fraction of time. . .". This part of the sentence is not clear. Please revise.

- Page 11, lines 15-16: We revised the sentence as follows: "Lightweight RTK/PPK-enabled multi-rotors may be more affordable than the senseFly eBee X with SODA 3D camera, but typically have a shorter battery life and subsequently lower areal coverage than fixed wings."

15. Figure 2: the font of the 3D point density images legend/scale is very small and difficult to read.

- In Figure 2, we increased the size of the text in the legend and scale.

<u>Comments from Anonymous Referee #2:</u>

1. **The use of drones for natural hazards damages evaluation is a well-known topic. It is important to point out that there is a special issue published on NHESS dedicated to UAV and natural hazards, I think that authors can find several interesting suggestions considering the published revision paper or the others. Another revision paper has been published by Gomez, C. and Purdie, H.: UAV- based Photogrammetry and Geocomputing for Hazards and Disaster Risk Monitoring – A Review, Geoenvironmental Disasters, 3, 1–11, 2016.**
    - We thank the referee for recommending these publications. We performed an extensive review of the literature and referenced what we believe to be the most relevant and applicable papers to our study.

2. **Page 3 line 20: the use of nadiral acquisition (both by drones or planes) can be critical in urbanized areas. In Giordan et al 2018, (see comment on chapter 4.2) the effect of damages caused by a flood was defined using a mixed approach based on drone and terrestrial acquisitions.**
    - We thank the referee for providing this context. In Section 4.2 of the original submission, we acknowledged that the addition of terrestrial images to drone-based aerial imagery has been shown to improve the 3D textured mesh model in urban study areas, and referred to Wu et al. (2018) as a demonstrative study. The scope of our study was to investigate the sole use of drone-based aerial imagery, and this imagery set was not nadir. As noted in Section 2.3, the 828 images were collected at an average pitch angle of 7 degrees off nadir.
    - To provide more detail about the obliquity of the imagery set, we modified the last sentence of Section 2.3 as such: "A total of 828 oblique images were captured. The median image pitch angle was 7.35 ° off nadir (3.55 ° interquartile range), with a minimum and maximum of 1.22 ° and 11.83 °, respectively".

3. **Page 4 line 15 "The RTK/PPK image georeferencing capabilities of the drone replaced the need for ground control points (GCPs), which are not practical to distribute and survey in an emergency mapping context." This is not correct. The RTK/PPk correction improves the accuracy of images acquisition points. The number and the needs of GCPs depend on the required accuracy of the SFM results. During the mission planning, it is possible to have an estimation of final accuracy and decide if GCPs are required or not. For fast acquisitions, often GCPs are not required, but for a pre-event acquisition, the required accuracy should be high, and I do not think that it is possible to avoid GCPs.**
    - We agree with the referee that GCPs can and should be used for pre-disaster mapping to maximize the geospatial accuracy of the data. We retain our position that GCPs are not practical to use for emergency (i.e., post-disaster) mapping. We used PPK corrections instead of GCPs because of the applicability of this georeferencing method to both pre- and post-disaster mapping.
    - To communicate the important point the referee has made, we modified this paragraph in Section 2.2 as such: "A senseFly eBee Plus drone with real-time kinematic (RTK)/post-processed kinematic (PPK) functionality and senseFly Sensor Optimised for Drone

Applications (SODA) red-green-blue (RGB) 20-megapixel camera were used to collect imagery. The RTK/PPK image georeferencing capabilities of the drone replaced the need for ground control points (GCPs), which are not practical to distribute and survey in an emergency (i.e., post-disaster) mapping context. It is important to note that, for pre-disaster mapping, GCPs should be used to maximize geospatial accuracy. Hugenholtz et al. (2016) demonstrate the improvement in DSM vertical accuracy when using a non-RTK senseFly eBee with GCPs compared to an RTK-enabled senseFly eBee without GCPs. For this pre-disaster mapping exercise in downtown Victoria, we chose to use RTK/PPK image georeferencing because this method is also applicable to post-disaster mapping. One of our objectives was to assess the geospatial accuracy of the pre-disaster data, which has implications for the use of RTK/PPK-enabled drones for post-disaster mapping and change detection applications."

4. **Page 6 line 10: In my experience, this is not the correct way to operate. The first step is the check of the right alignment of surveys. This can be done in particular using large plane areas (like car parking). Then you can compare buildings or other structures. The validation of the right position of DTM is mandatory to be sure that all used DSM are correct form the geodetic point of view. In an exercise like the one presented by authors, they could easily use as a sequence of Ground checkpoints to assure the accuracy of the obtained DSM. These checkpoints can be acquired using natural or artificial elements like (manholes) also after the UAV acquisition. To be rigorous, authors should present a more detailed study of the accuracy of the obtained DSM. This is a crucial point because the accuracy of the DSMs comparison is a function of the accuracy of used DSMs.**
   - We thank the referee for making this critical suggestion. We modified the vertical accuracy assessment by replacing the LiDAR checkpoints with 47 ground-surveyed (total station) checkpoints located on sewer manhole covers throughout the study area. These ground checkpoints follow the guidelines for vertical checkpoints as outlined in the 2015 ASPRS Positional Accuracy Standards for Digital Geospatial Data (ASPRS, 2015).
   - The modifications to the vertical accuracy assessment are reflected in changes to Section 2.5, Section 3.1, Section 4.1, Figure 1, Table 1, and Table 2.

5. **Chapter 2.6 it is not clear which is the goal of this chapter. Using nadiral images for facades is not correct, and this is not a novelty. Authors should clarify better if the final goal is the identification of damages comparing the geometry of roofs or the study of facades.**
   - To clarify our goal, we added the following text to the beginning of Section 2.6: "In addition to geospatial accuracy, we wanted to assess the quality of building representation in the drone-derived 3D data. This assessment would have implications on the usability of the 3D data for identifying damages to building roofs and facades".
   - As described in our response to Comment #2, the imagery set was not nadir.

6. **Authors should present the metadata of 2013 LiDAR before using it as a benchmark like the number of acquired points per meters, the accuracy of the survey, and the density of DSM point cloud. In particular, the DSM density is an important data. If the LiDAR density is not**

adequate, how authors can be sure that they comparing two points acquired in the same position or they are comparing a surveyed point and an artifact?

- Please refer to our response to Comment #4, where we modified the vertical accuracy assessment by using 47 ground checkpoints instead of the LiDAR checkpoints.

7. **Chapter 4.1 the presented "key lesson 1" is quite trivial. Authors presented obvious data for people familiar with LiDAR and drones DSM. Several critical issues are quite evident in this chapter: the most critical point is the a priori definition of LiDAR resolution and accuracy using García-Quijano et al. (2008). The final resolution of LiDAR surveys is a function of many parameters, like the point density, the flight velocity, the post processing accuracy, and many others. In this paper, authors never mentioned the characteristics of the available LiDAR survey. Another important element is that without the acquisition of checkpoints, authors are not able to define the accuracy of their UAV DSM. I think that this lack of information cannot be accepted in a scientific paper.**
    - We thank the referee for identifying the improvement that should be made to our reference for piloted LiDAR vertical accuracy. We removed García-Quijano et al. (2008) as the reference in Section 4.1 and Table 2. Instead, we used the 47 ground checkpoints to calculate the $RMSE_z$ of the LiDAR DSM generated using the piloted LiDAR data from our study area. We then used the $RMSE_z$ of the LiDAR DSM to modify Section 4.1 and Table 2. Additionally, we added the LiDAR metadata to Section 4.1.

8. **Page 10, line 5. The presence of differences in the geometry of several houses in the studied area could be useful for better development of the DSM comparison methodology. Using the comparison of DSM an images to check the first results, authors can be able to distinguish damages from building modifications. An improvement of the presented approach and the definition of an effective methodology for the recognition of damages can be an essential add value for this work, and it can also reduce the need of a continuous update of the DSM, which can generate a strong improvement of cost with a limited benefit. The only real result presented in chapter 4.1 is the difference between the results obtained by pix4d using the "rapid" and "full" point cloud. In my opinion, this cannot be considered an adequate result.**
    - If we are understanding this comment correctly, then the referee is suggesting we develop a methodology to distinguish between damaged buildings and modified buildings in the DoD. This is an excellent suggestion that would indeed contribute to reduced costs and time associated with continuously updating a pre-disaster DSM. If our interpretation of the referee's comment is correct, then we believe we do not have sufficient data for the proposed analysis. As shown in Figure 1b, the changes during the 5 years between the LiDAR (2013) and drone (2018) data acquisitions include new construction, structure removal, and parking lot excavation. The buildings that underwent new construction and structure removal could serve as examples of "modified buildings" in the referee's proposed analysis. However, our data lack examples of "destroyed buildings". Therefore, we believe we cannot perform what we interpret as the proposed analysis. However, we added the following to the end of Section 4.1: "To reduce costs and time associated with continuously updating a pre-

disaster DSM, future research should focus on developing methodologies to distinguish between construction-modified and disaster-damaged buildings in a DoD".

9. **Chapter 4.2 the presented "key lesson2" is focused on an interesting point. The nadiral acquisition of an urbanized area is not enough for the correct reconstruction of facades. Giordan et al. (Giordan, D., Notti, D., Villa, A., Zucca, F., Calò, F., Pepe, A., Dutto, F., Pari, P., Baldo, M., and Allasia, P.: Low cost, multiscale and multi-sensor application for flooded areas mapping, Nat. Hazards Earth Syst. Sci., 18, 1493-1516, 2018) published a multi-scale approach aimed to detect and measure damages on facades. The approach is different, but the topic is important for a correct estimation of damages. One of the problems of this article is the organization. If the authors want to analyze facades, they have to introduce this topic in advance and propose a possible methodology. The publication of a sequence of well-known limitations cannot be considered sufficient for an international scientific journal like NHESS.**
    - We strongly disagree with the referee's comment. We believe our research is novel because this is the first government-approved drone mapping mission over a major Canadian city. This was a multi-stakeholder effort that included the municipal emergency management office, federal aviation authority, and air traffic control. In their review paper concerning RPAS for natural hazards monitoring and management, Giordan et al. (2018) recommend that future research should "propose faster and automated approaches. In particular during emergencies, the time required for RPAS data set processing is an important element that should be carefully considered". Giordan et al. (2018) also recommend that, "In the following years, it would be desirable to witness the transfer of best practices in the use of RPASs be then from the research community to government agencies (or private companies) involved in the prevention and reduction of impacts of natural hazards. The scientific community should contribute to the definition of standard methodologies that can be assumed by civil protection agencies for the management of emergencies".
    - Consistent with the recommendations of Giordan et al. (2018), we present and evaluate a legal and plausible scenario. This is evidenced by our description of the multi-stakeholder coordination (Section 1.2), our use of the only legally approved drone for urban overflight in Canada to date (Section 1.2), our gridded flight plan for efficiency (as opposed to circular flights around individual buildings) (Section 1, Section 2.2), our use of PPK image georeferencing (as opposed to GCPs) (Section 2.2), and our examination of "rapid" image processing (Section 2.4, Section 4.1). By constraining our study to comply with the legal and logistical practicalities of pre- and post-disaster mapping in a major Canadian city, we believe our results have implications on the usability of the regulatory-approved drone for assisting in rescue and damage assessment activities. Specifically, the results inform the federal aviation authority (Transport Canada) of the limitations of this drone and camera configuration, and we suggest an equally safe alternative for legal approval (Section 4.2, Section 5). We also provide evidence-based lessons/best practices for practitioners such as emergency management offices. These best practices pertain to drone hardware (e.g., tilting cameras for 3D mapping [Section 4.2] and RTK/PPK georeferencing for change detection applications [Section 4.1]), data collection (e.g., takeoff and landing locations [Section 2.3] and up-to-date DSMs [Section

4.1]), and data processing (e.g., “rapid” processing for sub-meter building collapse detection [Section 4.1]).

- Additionally, by revising the accuracy assessment as recommended by the referee, we believe we provide a more rigorous analysis of the drone and LiDAR DSM accuracies.

References:

American Society for Photogrammetry and Remote Sensing (ASPRS): ASPRS Positional Accuracy Standards for Digital Geospatial Data, Photogramm. Eng. Remote Sens., 81(3), 1–26, doi:10.14358/PERS.81.3.A1-A26, 2015.

García-Quijano, M. J., Jensen, J. R., Hodgson, M. E., Hadley, B. C., Gladden, J. B. and Lapine, L. A.: Significance of Altitude and Posting Density on Lidar-derived Elevation Accuracy on Hazardous Waste Sites, Photogramm. Eng. Remote Sens., 74(9), 1137–1146, doi:10.14358/PERS.74.9.1137, 2008.

Giordan, D., Hayakawa, Y. S., Nex, F. and Tarolli, P.: Review article: the use of remotely piloted aircraft systems (RPASs) for natural hazards monitoring and management, Nat. Hazards Earth Syst. Sci., 18(4), 1079–1096, doi:10.5194/nhess-18-1079-2018, 2018.

Wu, B., Xie, L., Hu, H., Zhu, Q. and Yau, E.: Integration of aerial oblique imagery and terrestrial imagery for optimized 3D modeling in urban areas, ISPRS J. Photogramm. Remote Sens., 139, 119–132, doi:10.1016/j.isprsjprs.2018.03.004, 2018.

Pre-disaster mapping with drones: an urban case study in Victoria, BC, Canada

Maja Kucharczyk, Chris H. Hugenholtz

Department of Geography, University of Calgary, Calgary, AB T2N 1N4, Canada

Correspondence to: Maja Kucharczyk (maja.kucharczyk@ucalgary.ca)

Abstract. We report a case study using drone-based imagery to develop a pre-disaster 3D map of downtown Victoria, British Columbia, Canada. This represents the first drone mapping mission over an urban area approved by Canada's aviation authority. The goal was to assess the quality of the pre-disaster 3D data in the context of geospatial accuracy and building representation. The images were acquired with a senseFly eBee Plus fixed-wing drone with real-time kinematic/post-processed kinematic functionality. Results indicate that the spatial accuracies achieved with this drone would allow for sub-meter building collapse detection, but the non-gimbaled camera was insufficient for capturing building facades.

1 Introduction

Currently, 55 % of the global population resides in urban areas, and this is projected to increase to 68 % by 2050 (United Nations, 2018). ~~As the global population increases and a greater proportion is concentrated in urban areas,~~Increasing global population and urbanization (particularly in vulnerable areas) are factors that can contribute to increased death and destruction by natural hazards like earthquakes and tropical cyclones~~ will rise~~. In addition to initiatives such as increased quality of construction, alarm systems, and proximity to rescue services, ~~Pre~~pre-disaster mapping can help increase a city's resilience against disasters (Pu, 2017). Combining vector layers, digital elevation models, and aerial/satellite imagery, maps are powerful tools for mitigation and preparedness before a disaster strikes (Pu, 2017). Copernicus Emergency Management Service (Copernicus EMS), one of the main contributors of disaster management maps globally, has used pre-disaster data to produce thousands of reference maps (showing territories and assets), pre-disaster situation maps (showing hazard levels, evacuation plans, and modeling scenarios), and damage grading maps (showing distribution and level of damage to buildings and infrastructure). Copernicus EMS generates damage grading maps by visually comparing pre- and post-disaster satellite imagery (Copernicus EMS, 2017). Nearby debris is used as a proxy for building structural damage, as building facades cannot be directly examined (Copernicus EMS, 2017).

The leading cause of death in an earthquake is building collapse (Moya et al., 2018). Remote sensing can potentially assist first responders in rapidly locating collapsed buildings to prioritize search and rescue efforts (Moya et al., 2018). However, clouds and access to satellite imagery can cause delays in analysis and preclude the traditional 2D approach from being useful for search and rescue. Furthermore, partial building collapse, which can trap and kill victims, generates lower amounts of debris than complete collapse, so the dependence on debris as a proxy for collapse becomes less reliable. Research has shown that 2.5D data can build upon the traditional 2D approach and increase the reliability of collapse detection by observing elevation changes over buildings. Following the 2016 Kumamoto earthquake in Japan, Moya et al. (2018) detected collapsed buildings using pre- and post-earthquake light detection and ranging (LiDAR) digital surface models (DSMs). For each building, they calculated the average height difference between the DSMs and manually set a threshold value to detect collapse – this technique had a Cohen's kappa coefficient and overall accuracy of 0.80 and 93 %, respectively (Moya et al., 2018). Pre-event LiDAR data, however, can often be outdated, leading to false detections, or unavailable, especially in less-developed parts of the world. Post-event LiDAR data may be difficult to rapidly obtain. To address these operational challenges, drones are an alternative platform for acquiring 2.5D and 3D data, and when stored locally for emergency mapping, can be used to rapidly acquire data. Drone-derived aerial imagery, when paired with structure-from-motion ~~(SfM)~~multiview-stereo image processing software, can be used to generate sub-decimeter resolution orthomosaics, DSMs, and photorealistic 3D models in the form of colorized point clouds and textured meshes.

Drone-based mapping can also potentially support longer-term needs assessments and reconstruction monitoring by surveying building damage levels. The traditional 2D approach with satellite imagery only provides information about building roofs and nearby debris, and previous research has shown that oblique perspectives of building facades are valuable for discerning between lower grades of building damage (Kakooei and Baleghi, 2017; Masi et al., 2017). Previous studies have conducted drone-based 3D mapping of buildings following a disaster. The motivation is to complement ground-based building damage assessments – cataloging the exterior damages in 3D can support the planning/prioritizing of subsequent, more thorough ground-based assessments (Vetrivel et al., 2018), and the planning/monitoring of reconstruction. Previous studies (e.g., Fernandez Galarreta et al., 2015; Cusicanqui et al., 2018) have reported that damage features such as deformations, cracks, debris, inclined walls, and partially collapsed roofs are identifiable in drone-based 3D point clouds and mesh models. These findings demonstrate that drone 3D data are capable of supporting post-disaster activities. However, previous studies have been limited to drone-based 3D mapping: (i) a single building (Achille et al., 2015; Meyer et al., 2015), (ii) small, historic villages (Vetrivel et al., 2015; Dominici et al., 2017; Calantropio et al., 2018; Cusicanqui et al., 2018; Vetrivel et al., 2018), or (iii) modern cities, but without focus on the quality of building representation in the 3D data (Cusicanqui et al., 2018; Vetrivel et al., 2018). It is important to understand how drone-based 3D data would reconstruct a cityscape, particularly with a grid-based survey to capture multiple city blocks in a single flight. This flight pattern would balance areal coverage with 3D reconstruction quality. The dense spacing of buildings and the presence of high-rises in an urban scene create considerable potential for camera occlusion and may result in 3D mesh defects such as inaccurate shapes, holes, and blurred textures (Wu et al., 2018).

In addition to issues with photogrammetry, it is challenging to collect drone data over dense, urban areas due to ~~airspace~~ aviation regulations that were designed to protect public safety. As such, in a disaster context, drone data over cities have generally been collected in the post-disaster phases, when destruction is widespread and these data are in high demand. With historic emphasis on data collection in the post-disaster phases, it is important not to detract from pre-disaster mapping.

Pre-disaster mapping not only provides baseline data from which to assess changes, but is also a crucial exercise that enables emergency management actors to establish operational protocols to maximize the effectiveness of drones in emergencies. These protocols pertain to drone hardware/software, data collection, data processing, and data analysis.

We present a case study of pre-disaster mapping with a drone in Victoria, British Columbia, Canada. Victoria has at least a 30 % probability of experiencing a significantly damaging earthquake in the next 50 years (AIR Worldwide, 2013). A 2016 report on the seismic vulnerability of Victoria ~~conducted~~ presented a risk assessment for all buildings (13,330 buildings) in Victoria under various earthquake scenarios and levels of ground shaking (VC Structural Dynamics Ltd, 2016). The report concluded that 30 % of the buildings (3,936 buildings) have a high seismic risk, meaning they have at least a 5 % probability of complete damage in a 50-year period (VC Structural Dynamics Ltd, 2016). This pre-disaster mapping exercise was undertaken for City of Victoria's Emergency Management Division and in partnership with GlobalMedic, a Canadian disaster relief charity. This was the first Transport Canada-approved drone ~~flight~~ mapping mission over a major Canadian city. We were restricted by regulations to use a specific platform, a 1.1 kg senseFly eBee fixed-wing drone. The overarching goal of this case study was to assess the quality of the drone data that we were able to obtain in a manner adhering to federal regulations.

1.1 Objectives

The first objective was to assess the geospatial accuracy of the drone data. Geospatial accuracy is important for change detection applications, as it relates to the quality of registration between pre- and post-disaster datasets. This was done by first assessing the vertical accuracy of the drone DSM using ~~339 airborne LiDAR~~47 ground-surveyed checkpoints. Then, a LiDAR DSM was subtracted from the drone DSM to visually assess the horizontal alignment of rooftops as a qualitative measure of horizontal accuracy. The second objective was to assess the quality of 3D building representation. The only legally approved drone for this flight presents challenges for 3D mapping of cities, as it is a fixed-wing drone with a non-gimbaled camera. Research has shown that high camera tilt angles, which are not achievable with the regulatory platform for this flight, will result in higher reconstruction density (less data gaps) and precision of points on building facades than lower camera tilt angles (Rupnik et al. 2015). The quality assessment of 3D building representation was done by visually assessing the drone 3D textured mesh, and using Google 3D (i.e., "3D Buildings" layer in Google Earth) as a reference for building appearance. Additionally, we applied a method previously used on post-disaster, drone-derived 3D point clouds to quantify data gaps on sample building facades.

1.2 Regulatory background

Transport Canada is the aviation authority that regulates drone operations in Canadian airspace. The current regulations require case-by-case permission for drone flights in urban areas. Permission is sought by submitting an application for a Special Flight Operations Certificate, where the applicant must demonstrate sufficient ground/flight training, standard operating procedures, emergency procedures, drone maintenance procedures, and more. Additionally, coordination with air traffic control (Nav Canada) was required to perform the flight, as downtown Victoria is within controlled airspace, with nearby airports, heliports, and seaplane bases causing high-density air traffic. The only approved drone for this flight was a senseFly eBee, of which the “Plus” model was used for its higher georeferencing accuracy. The senseFly eBee Plus is a 1.1 kg, 1.1 m wingspan, fixed-wing drone made of lightweight expanded polypropylene foam, carbon fiber, and composite materials. The ~~two~~ eBee Classic, SQ, and Plus models are the lightest on the list of compliant drones for Transport Canada, which includes drones meeting federal safety and quality standards. For this flight, the senseFly eBee drone was approved by Transport Canada due to its light weight and ability to glide to a landing.

2 Methods

2.1 Flight area

The drone flight covered a 1 km^2 area of downtown Victoria, BC, Canada. The western half and eastern half of the flight area covered parts of the Historic Commercial District (HCD) and Central Business District (CBD), respectively, resulting in image capture over a diversity of building types and heights. The HCD contains an undulating streetscape with low- to mid-rise, brick- and stone-facade buildings alternating between one and five stories, including boutique hotels, heritage buildings, businesses, and offices (CoV, 2011). The CBD contains high-density, mid- to high-rise commercial and residential buildings (CoV, 2011). The building heights within the flight area ranged from 2–55 m, and street widths varied between 7–24 m.

2.2 Drone hardware and flight planning

A senseFly eBee Plus drone with real-time kinematic (RTK)/post-processed kinematic (PPK) functionality and senseFly Sensor Optimised for Drone Applications (SODA) red-green-blue (RGB) 20-megapixel camera were used to collect imagery. The RTK/PPK image georeferencing capabilities of the drone replaced the need for ground control points (GCPs), which are not practical to distribute and survey in an emergency (i.e., post-disaster) mapping context. It is important to note that, for pre-disaster mapping, GCPs should be used to maximize geospatial accuracy. Hugenholtz et al. (2016) demonstrate the improvement in DSM vertical accuracy when using a non-RTK senseFly eBee with GCPs compared to an RTK-enabled senseFly eBee without GCPs. For this pre-disaster mapping exercise in downtown Victoria, we chose to use RTK/PPK image georeferencing because this method is also applicable to post-disaster mapping. One of our objectives was to assess the geospatial accuracy of the pre-disaster data, which has implications for the use of RTK/PPK-enabled drones for post-disaster mapping and change detection applications.

The drone’s PPK mode was used, with correction data obtained from the Natural Resources Canada (~~NRCAN~~NRCan) Canadian Active Control System (Albert Head reference station, 10 km from flight area). SenseFly eMotion (v3) software (eMotion) (senseFly, 2018) was used to plan the flight. The flight was grid-based, composed of orthogonal flight lines running non-parallel with streets (i.e., approximately 45 ° offset). The addition of perpendicular flight lines and the orientation of the grid were used to increase image coverage of building facades. The imagery frontal and lateral overlap were set to 75 %, and the flight altitude was 120 m above ground level (AGL).

2.3 Drone image acquisition

The flight was conducted on June 14, 2018. The operations took place in the morning for increased safety, i.e., low air traffic. However, the ideal flight time would be solar noon to minimize shadows from buildings. The ground control station was set up on a parkade rooftop within the flight area. The parkade, surrounded by relatively low buildings and an open courtyard, allowed for unobstructed takeoff/landing, visual line of sight, and radio signal between the drone and ground control station. A total of 828 oblique images were captured~~,~~. ~~with~~ The median image pitch angle was ~~s averaging~~ 7.35 ° off nadir (3.55 ° interquartile range), with a minimum and maximum of 1.22 ° and 11.83 °, respectively.

2.4 Image processing

The images were processed using a high-performance computer (Intel® Core™ i9-7900X CPU @ 3.30 GHz with 64 GB RAM and NVIDIA GeForce GTX 1080 GPU). First, eMotion was used for PPK processing by incorporating raw global navigation satellite system (GNSS) observations from the reference station and drone to refine the image geotags. The geotagged images were processed using Pix4Dmapper Pro (v4.3.27) (Pix4D) (Pix4D, 2018), a structure-from-motion multiview-stereo (SfM-MVS) software. SfM-MVS generally consists of the following steps. First, computer vision algorithms search through each image to identify “features” – that is, pixel sets that are robust to changes in scale, illumination, and 3D viewing angle (Westoby et al., 2012). Next, the features are assigned unique “descriptors”, which allow for the same features to be identified across multiple images, and for the images to be approximately aligned (Westoby et al., 2012). This initial image alignment is iteratively optimized via bundle adjustment algorithms, the output of which is a sparse 3D point cloud of feature correspondences (Westoby et al., 2012). Multiview-stereo algorithms then densify the sparse point cloud, typically by two or more orders of magnitude (Westoby et al., 2012). The dense point cloud is then used to generate a 3D textured mesh, which is a triangulated surface that is textured using the original images. The dense point cloud is also used to generate a DSM. The DSM and images are used to generate an orthomosaic.

For the first objective of assessing the geospatial accuracy of the drone data, five DSMs were generated. Each DSM had increasingly computationally intensive parameters, resulting in an increasingly higher processing time. These various combinations were used to assess the differences in vertical accuracy achieved with “rapid” and “slow” processing, ranging in total processing time from 0.50–8.14 h. This comparison has important implications on the applicability of a drone-based DSM for rapid building collapse detection, where time is a major factor. Four “rapid” DSMs were generated in Pix4D using values of 1/8, 1/4, 1/2, and 1 for the image scale parameters (Step 1: keypoints image scale and Step 2: image scale), and low density for the point cloud. One “slow” DSM was generated using a value of 1 for the image scale parameters, and optimal (medium) density for the point cloud. All 5 DSMs were generated using 3 minimum matches, noise filtering, “sharp” surface smoothing, and inverse distance weighting interpolation. For the second objective of assessing 3D building representation, the 3D textured mesh was generated in Pix4D using a value of 1 for the image scale parameters, optimal (medium) density for the point cloud, 3 minimum number of matches, and high resolution for the textured mesh. A medium-resolution mesh was also generated for comparison to the high-resolution mesh.

All Pix4D data outputs had a spatial reference of Universal Transverse Mercator (UTM) Zone 10N, North American Datum of 1983 (Canadian Spatial Reference System) (NAD83 [CSRS]), using the Canadian Geodetic Vertical Datum of 2013 (CGVD2013) for orthometric heights relative to the Canadian Gravimetric Geoid model of 2013 (CGG2013~~(~~, 2010.0 epoch) ~~geoid model~~. The DSMs were assessed for geospatial accuracy, while the point cloud and textured meshes were used to assess 3D building representation in terms of geometry and texture.

2.5 Geospatial accuracy assessment

To be useful for change detection, such as DSM differencing for building collapse detection (e.g., Moya et al., 2018), the drone data must be geospatially accurate. Otherwise, misregistration of the drone data with pre- or post-event data may cause false detections. Therefore, the geospatial accuracy of each drone DSM was assessed using ~~a 2013 LiDAR point cloud~~47 ground-surveyed checkpoints ~~as a reference dataset~~. The vertical accuracy assessment was conducted using recommendations from the 2015 American Society for Photogrammetry and Remote Sensing (ASPRS) Positional Accuracy Standards for Digital Geospatial Data (ASPRS, 2015). ASPRS (2015) recommend vertical checkpoints to be ground-surveyed and located on flat or uniformly sloped (≤ 10 % slope), open terrain, away from vertical artifacts and abrupt elevation changes. The checkpoints used in this accuracy assessment were collected using a total station, and represent sewer manhole covers located on paved roads throughout the study area.~~The vertical accuracy assessment was conducted using recommendations from the 2015 American Society for Photogrammetry and Remote Sensing (ASPRS) Positional Accuracy Standards for Digital Geospatial Data (ASPRS, 2015). ASPRS (2015) note that kinematic checkpoints (surveyed from a moving platform) can be used as supplemental reference data, but static checkpoints should be used for the main accuracy assessment. Due to unavailability of ground survey data, the accuracy assessment used LiDAR data as the reference. The LiDAR data were acquired in 2013, had an average point spacing of 0.31 m, and had the same spatial reference as the drone data. The vertical error of each drone DSM was calculated using LiDAR checkpoints located on rooftops only, since the motivation was to assess the usability of the drone DSM for building collapse detection. To extract checkpoints from the LiDAR point cloud, first, 5000 points were randomly subsampled using CloudCompare (v2.9.1). From those 5000 points, only points corresponding to rooftops were retained. To avoid selecting checkpoints on rooftops that were not present during the 2013 LiDAR data collection, a 2013 satellite image was viewed in Google Earth and compared to the drone orthomosaic to determine buildings common to both datasets. ASPRS (2015) recommend vertical checkpoints be located on flat or uniformly sloped (≤ 10 % slope), open terrain, away from vertical artifacts and abrupt elevation changes. Therefore, the final selection of LiDAR checkpoints included only those on flat rooftops and away from edges and roof objects. A total of 339 LiDAR checkpoints were retained. Each LiDAR~~Each checkpoint z-coordinate (~~z_{LiDAR}~~z_{ref}) was subtracted from the corresponding drone DSM value (z_{drone}) to calculate errors (z_{drone} – ~~z_{LiDAR}~~z_{ref}). A Shapiro-Wilk test (α level of 0.05) and a visual inspection of the histogram, normal Q-Q plot, and box plot indicated that the errors followed a normal distribution. Therefore, vertical accuracy was calculated as the vertical root mean squared error ($RMSE_z$) following Eq. (1):

$$RMSE_z = \sqrt{\frac{1}{n}\sum_{i=1}^{n}(z_{i(drone)} - z_{i(\cancel{LiDAR}ref)})^2}, \quad (1)$$

where $z_{i(drone)}$ is the value of the ith cell from the drone DSM, $z_{i(\cancel{LiDAR}ref)}$ is the z-coordinate of the corresponding ~~LiDAR point~~checkpoint, and the total number of observations is represented by n (ASPRS, 2015). To visually assess the horizontal accuracy of the drone data, a DSM of difference (DoD) was generated by subtracting a LiDAR DSM from the drone DSM. The LiDAR data were collected in 2013, and had an average point spacing of 0.31 m. To generate the DoD, ~~First~~first~~,~~ the LiDAR point cloud was interpolated into a 0.31 m DSM in ESRI ArcMap (v10.5.1) (ESRI, 2018) using inverse distance weighting interpolation and linear void fill. The LiDAR DSM was then subtracted from the "slow" drone DSM to calculate a 0.31 m DoD ($DoD = DSM_{drone} - DSM_{LiDAR}$). The DoD was used to visually assess the horizontal alignment of roofs as a qualitative measure of horizontal accuracy.

2.6 Assessment of building geometry and texture

In addition to geospatial accuracy, we wanted to assess the quality of building representation in the drone-derived 3D data. This assessment would have implications on the usability of the 3D data for identifying damages to building roofs and facades. The medium- and high-resolution textured meshes were visually assessed for quality of building representation in terms of geometry and texture. Eight sample buildings ranging in geometrical complexity were segmented from each mesh using CloudCompare (v2.9.1) (CloudCompare, 2018) and were visually compared. Google 3D (i.e., Google Earth layer "3D Buildings") served as a reference for building appearance. The Google 3D layer was photogrammetrically derived using nadir and 45 ° aerial imagery that was collected with a multi-camera system in 2014. To support the visual assessment, each sample building was segmented from the dense point cloud, and each building point cloud was colored by 3D point density using CloudCompare. To further investigate geometrical and textural distortions within the mesh, the dense point cloud was used to quantify data gaps on building facades (i.e., regions of facades without points). The procedure generally followed Cusicanqui et al. (2018), who assessed the completeness of drone-based point clouds of post-earthquake study areas in Taiwan and Italy. Using CloudCompare, six sample facades were segmented from the dense point cloud. The Rasterize tool was used to project the points of each segmented facade onto a 0.50 m grid, with the projection plane parallel to the facade. Then, a 0.50 m raster was generated, showing the number of 3D points in each cell. For each raster, the percentage of facade data gaps was calculated by dividing the number of empty cells by the total number of cells. To support the data gap assessment, the sample facades were also segmented from the high-resolution mesh using CloudCompare.

3 Results

3.1 Geospatial accuracy of drone DSM

The vertical error of each drone DSM was calculated using ~~339 randomly selected LiDAR~~47 ground-surveyed checkpoints located on ~~flat roofs and away from edges and roof objects~~sewer manhole covers. For the "slow" DSM, errors ranged from ~~-~~0.~~09~~03–0.~~20~~ 13 m (Fig. 1a). The mean vertical error was 0.~~06~~ 08 m, with a standard deviation of 0.~~04~~ 02 m (Fig. 1a), demonstrating the drone DSM tended to overestimate the elevation of ~~rooftops~~the ground surface. Table 1 shows the $RMSE_z$ values of the "slow" DSM and the 4 "rapid" DSMs. $RMSE_z$ decreased as total processing time increased (Table 1). The DSM generated in the least amount of time, 0.50 h, had an $RMSE_z$ of 0.16 m, which is 0.~~09~~ 08 m higher than the $RMSE_z$ for the "slow" DSM, generated in 8.14 h (Table 1). The horizontal accuracy of the "slow" DSM was visually assessed by calculating a DSM of difference (DoD = DSM_{drone} – DSM_{LiDAR}) (Fig. 1b). The DoD shows blue tints for elevation overestimations and red tints for elevation underestimations by the drone DSM (Fig. 1b). A 2013 satellite image was viewed in Google Earth and compared to the drone orthomosaic to determine buildings common to both datasets. Figure 1b identifies 16 buildings with large regions of contiguous DSM differences. These contiguous DSM differences are due to changes that occurred between the 2013 LiDAR and 2018 drone data acquisitions, such as new construction, structure removal, and parking lot excavation (Fig. 1b). For the rest of the DoD, the red and blue cells mostly correspond to changes in vegetation, and inconsistencies in building footprint edges between the drone and LiDAR DSMs (Fig. 1b). Building outlines appear mostly blue, and don't appear weighted more heavily in one direction (Fig. 1b), suggesting no major horizontal offset of the drone DSM relative to the LiDAR DSM. With a 0.31 m average point spacing, it is possible that the LiDAR point cloud did not sample roof edges, resulting in slightly smaller building footprints in the LiDAR DSM than the drone DSM. Building footprint edge differences could also be due to inaccurate geometry from drone-based photogrammetry.

3.2 Building representation: mesh resolution and data gap assessment

The appearance of buildings varied considerably between the medium- and high-resolution 3D meshes. Figure 2 shows eight sample buildings represented by the dense point cloud (colored by 3D point density), both meshes, and Google 3D as a reference. Both meshes were generated using the settings described in § 2.4, with only the mesh resolution setting varying. For each building, the point density is higher on roofs than facades, and data gaps (i.e., regions of zero points) are visible within facades (Fig. 2). The medium-resolution mesh has visibly poorer reconstruction of building geometry and, subsequently, more deformations in texture than the high-resolution mesh (Fig. 2). This was expected, as each medium-resolution building contains only 4–5 % of the vertices/faces of its high-resolution counterpart. Figures 2a–2d show heritage buildings with complex geometry: Victoria City Hall (Fig. 2a), St. John the Divine Anglican Church (Fig. 2b), Alix Goolden Performance Hall (Fig. 2c), and St. Andrew's Cathedral (Fig. 2d). Smaller architectural features common to these heritage buildings, such as gabled entrances, dormer windows, conical roofs, spires, and towers are better resolved in the high-resolution mesh (Fig. 2a–d). For these buildings, as well as buildings with simpler geometry (Fig. 2e–h), the high-resolution mesh shows higher linearity of facade, roof, and window edges. For the high-rise buildings (Fig. 2e–h), facades with widespread data gaps in the point cloud appear to protrude inward and outward in the meshes, and have severe textural distortions. For generally planar facades with regular sampling (e.g., the front-facing facades in Fig. 2e and 2f), the apparent geometrical and textural differences between the medium- and high-resolution meshes are less prominent. The 95–96 % lower density of vertices/faces in the medium-resolution mesh appears more robust to geometrical/textural distortions for buildings with simpler, planar geometry than those with complex geometry, provided there is adequate sampling. However, as demonstrated by the high-rise buildings (Fig. 2e-h), facades with widespread data gaps have severe distortions, regardless of mesh resolution.

~~Due to considerable improvements in building geometry and texture, the high-resolution textured mesh was assessed going forward.~~ As demonstrated by the point-density point clouds in Fig. 2, roofs were more densely and regularly sampled than facades, and some facades contained widespread gaps that resulted in severe distortions in the meshes. To further assess facade data gaps, particularly partial data gaps, six facades were segmented from the dense point cloud and high-resolution mesh. The 0.50 m point density raster and high-resolution mesh segmentation are shown for each facade in Fig. 3. Data gaps, represented by red cells, encompass 9–59 % of the facades (Fig. 3). For each facade, large regions of contiguous red cells in the point density raster appear attributed to distortions in the mesh (i.e., stretched texture and inwardly protruding geometry).

4 Discussion

4.1 Key lessons: drone geospatial accuracy and up-to-date, pre-disaster DSMs

For building collapse detection (e.g., Moya et al., 2018), drones can provide post-event DSMs that can be differenced with LiDAR or photogrammetrically derived pre-event DSMs. However, there are geospatial accuracy requirements to avoid artificial detections caused by the misregistration of pre- and post-event DSMs. As such, we conducted a vertical accuracy assessment of each drone DSM using ~~LiDAR checkpoints located on flat roofs only, as the goal was to assess the usability of the drone DSM for building collapse detection. Based on 339 checkpoints,~~47 ground-surveyed checkpoints. ~~the~~ The $RMSE_z$ of the "slow" drone DSM, generated in 8.14 h, was 0.~~07~~ 08 m, and the $RMSE_z$ of the most "rapid" drone DSM, generated in 0.50 h, was 0.16 m (Table 1). To assess the implications of the vertical accuracies, a level of detection (LoD) can be calculated to determine the threshold elevation difference that can be detected using pre- and post-disaster DSMs with known $RMSE_z$ values, following Eq. (2):

$$LoD = \pm 3 \times \sqrt{(RMSE_{z1})^2 + (RMSE_{z2})^2}, \quad (2)$$

where $RMSE_{z1}$ is the RMSE of the pre-disaster DSM, $RMSE_{z2}$ is the RMSE of the post-disaster DSM, and the multiplier, 3, represents the extreme tails of a normal probability distribution (Hugenholtz et al., 2013). Table 2 shows hypothetical DoDs, each generated with a different combination of pre- and post-disaster DSMs, and their resulting LoDs from Eq. (2). In Table 2, the $RMSE_z$ values for the "slow" and "rapid" drone DSMs were experimentally derived in this study. The $RMSE_z$ for piloted LiDAR (0.04 m) was calculated using the 2013 LiDAR DSM ~~was experimentally derived by García-Quijano et al.~~and 47 ground-surveyed checkpoints~~ (2008)~~ (Table 2). The LiDAR data were acquired with a Leica ALS70-HP sensor from an average flight altitude and speed of 1360 m AGL and 220 knots, respectively. The field of view and average swath width were 47 ° and 1240 m, respectively. The scan rate was 48.9 Hz, and the laser pulse rate was 370.6 kHz. ~~Based on 71 RTK-GNSS vertical checkpoints from a nearly level (approximately 3 % slope) study area covered by short grass, García-Quijano et al. (2008) calculated an RMSE$_z$ of 0.07 m for a triangulated irregular network (TIN) interpolated using a bare-earth LiDAR point cloud with an average point spacing of 0.61 m (Table 2).~~ The RMSE$_z$ for a non-RTK/PPK drone was experimentally derived by Hugenholtz et al. (2016) (Table 2). Based on 180 RTK-GNSS vertical checkpoints from a gravel pit, Hugenholtz et al. (2016) calculated an RMSE$_z$ of 2.144 m for a non-RTK/PPK senseFly eBee (no GCPs), and an RMSE$_z$ of 0.089 m for an RTK/PPK-enabled senseFly eBee (no GCPs) (similar to our RMSE$_z$ of 0.~~07~~08 m). For each hypothetical DoD in Table 2, the corresponding LoD value indicates that any elevation difference between -LoD and +LoD is likely due to error and cannot be interpreted as real. DoDs generated with one or more DSMs derived from a non-RTK/PPK drone (DoD5 and DoD6) had LoDs of 6.~~44~~43 m and 9.10 m (Table 2). For LoDs attributed to the use of non-RTK/PPK drones, buildings shorter than the LoDs cannot be assessed for collapse, and for assessable buildings, only DoD values exceeding the LoDs are likely to correspond to real collapse. The 6.~~44~~43 m and 9.10 m LoDs exceed the typical height of a single building story, suggesting that DoDs generated with non-RTK/PPK drones cannot be reliably used to detect partial collapse. Conversely, DoDs generated with one or more DSMs from an RTK/PPK drone (DoD1–4) had LoDs ~~of 0.30 m and 0.52 m~~ranging from 0.27–0.54 m, suggesting that these DoDs can be reliably used to detect partial collapse (Table 2). This includes DoD3 and DoD4, both generated using a "rapid" post-event drone DSM (Table 2). The use of the lowest image scale value (1/8) and lowest point density in Pix4D to generate the most rapid DSM in 0.50 h (Table 1) retained sub-~~decimeter~~ meter LoDs (0.49–0.54 m~~0.52 m~~) (Table 2). These results demonstrate that RTK/PPK-enabled drones are required for reliable building collapse detection, and rapid processing settings can be used.

Furthermore, the DoD showed buildings with large regions of contiguous DSM differences due to changes that occurred between the 2013 LiDAR and 2018 drone data acquisitions, such as new construction, structure removal, and parking lot excavation (Fig. 1b). This demonstrates that, for building collapse detection, it is necessary to maintain an up-to-date, pre-disaster DSM to avoid false detections. Victoria has an ever-changing downtown core, with rezoning and new developments to help accommodate significant population growth forecasted over the next 20~~–30~~ years (CoV, 2011). With constant new construction throughout growing cities like Victoria, it is important for municipalities to regularly update DSMs, such that changes in construction are not masked as disaster-induced destruction. To reduce costs and time associated with continuously updating a pre-disaster DSM, future research should focus on developing methodologies to distinguish between construction-modified and disaster-damaged buildings in a DoD.

4.2 Key lessons: drone mesh resolution and imaging platform

From an image processing standpoint, it was shown in § 3.2 that mesh geometry and texture are improved considerably from a medium-resolution to a high-resolution mesh (Fig. 2). This high-resolution mesh required more processing time, including subsetting the project into two, but these improvements justify the added time for virtual 3D damage assessment applications. For image collection, the deformed geometry and texture of buildings (Fig. 2 and 3) could be improved by collecting highly oblique images of facades in addition to nadir images of roofs and ground features. The average 7 ° camera pitch angle used in this case study was likely insufficient for capturing vertical and near-vertical faces, resulting in large point cloud data gaps and geometrical/textural distortions in the 3D mesh (Fig. 2 and 3). Using a higher camera angle (e.g., 30–45 ° off nadir) could make important improvements, for deformations in the 3D model could be mistaken for building damage. Rupnik et al. (2015) found that increasing the camera tilt angle resulted in a higher point density on building facades and higher 3D precision of points, and that the addition of oblique images to a nadir image set increased the vertical accuracy of points. This suggests that different hardware is required for 3D mapping of municipalities with small drones. Options include multi-rotor drones with gimbaled cameras that are capable of highly oblique image capture. However, ~~this challenges current regulations that only allow lightweight, fixed-wing drones to be flown over municipalities~~we suspect multi-rotor drones are less likely to be legally approved for urban overflight than fixed-wing drones. ~~To comply with current regulations, a~~A potential solution is to use a lightweight fixed-wing drone with a camera that tilts for oblique image capture. One commercially available option is the senseFly eBee X drone with a senseFly SODA 3D RGB camera, which captures one nadir image and two laterally oblique images per waypoint. The eBee X model became available in September 2018, after the data capture in this study. Lightweight RTK/PPK-enabled multi-rotors may be more affordable than the senseFly eBee X with SODA 3D camera, but ~~achieve a fraction of the flight time~~typically have a shorter battery life and subsequently lower areal coverage ~~of~~ than fixed wings.

It is important to note that a higher camera angle is not a panacea – higher camera tilt angles result in higher occlusions due to surrounding buildings, which contribute to lower point density on lower parts of facades (Rupnik et al., 2015). Moreover, point cloud gaps will persist on facades due to several factors: (i) occlusions caused by surrounding buildings, facade protrusions, and other objects, (ii) insufficient texture, (iii) highly reflective surfaces like glass, and (iv) poor image quality (Fonstad et al., 2013; Alsadik et al., 2014). Another potential solution is to obtain images of building facades from the ground. Wu et al. (2018) showed that drone-derived textured meshes of urban study areas in Germany and Hong Kong were improved with the integration of ground-based images. The meshes had increased geometric accuracy and improved texture (Wu et al., 2018). However, potential challenges to obtaining terrestrial images include added time, safety concerns, and limited access.

The data acquisition methods used in this study will need to be adapted to fit the conditions of different urban areas. For example, flight altitude will need to be adjusted to give a safe vertical clearance from the tallest building. If the terrain in the area is sloped, elevation data should be input to the flight planning software to keep the flight altitude constant. A grid of flight lines is recommended, although its orientation and image overlap will vary depending on factors such as building layout and density. In a post-disaster context, a takeoff and landing location may be difficult to locate and access due to widespread destruction. Weather conditions such as high winds and rain following storm events may pose challenges to the flying ability of lightweight drones. Atmospheric conditions such as haze and smoke limit optical sensors in imaging destruction. These factors are examples of considerations that should be made when adapting the data acquisition methodology in this study.

5 Conclusions

We presented a case study of drone-based pre-disaster mapping in downtown Victoria, BC, Canada. The objectives were to assess the quality of the data in terms of geospatial accuracy and 3D building representation. Using ~~339 airborne LiDAR checkpoints located on flat roofs~~47 ground-surveyed checkpoints, the $RMSE_z$ of the drone DSM was 0.~~07~~ 08 m. The DSM of difference (DoD = $DSM_{drone} - DSM_{LiDAR}$) showed complete roof overlap, suggesting adequate horizontal accuracy for change detection applications. For building collapse detection, we devise drones with RTK/PPK image georeferencing capabilities and up-to-date, pre-disaster DSMs are required to avoid false detections. Furthermore, image processing using "rapid" settings, as opposed to "slow" settings, reduced processing time from 8.14 h to 0.50 h, increased DSM $RMSE_z$ from 0.~~07~~ 08 m to 0.16 m, and increased DoD LoD from 0.~~30~~ 34 m to 0.~~52~~ 54 m. Though processing times were specific to our computing hardware, these differences demonstrate that "rapid" processing is capable of quickly generating DSMs that can reliably detect sub-meter building collapse. Conversely, ~~theoretical~~ hypothetical DoDs derived from one or more non-RTK/PPK drone DSMs have LoDs too high (i.e., > 6 m) to reliably detect partial building collapse. These results suggest that RTK/PPK-enabled drones and "rapid" image processing are most suitable for rapid building collapse detection with drones.

For virtual building damage assessment with drone-derived 3D textured meshes, it was shown that a high-resolution mesh, containing 95–96 % more vertices/faces than a medium-resolution mesh, visually improved building geometry and texture, especially for heritage buildings with complex geometries and small architectural features. However, neither mesh resolution was able to cope with large point cloud gaps on building facades. These data gaps were shown to correspond with severely distorted geometry and texture in the mesh. Therefore, for future drone-based pre- and post-disaster 3D mapping of municipalities, different hardware would be required. The ability to capture highly oblique images is paramount for virtually reconstructing building facades. Options include a multi-rotor drone with a gimbaled camera. However, ~~follow-up studies with lightweight multi-rotor drones will not be possible without modification to existing airspace regulations~~we suspect that lightweight multi-rotors are less likely to be approved for mapping missions in urban areas. Therefore, we suggest a follow-up study with a senseFly eBee X with SODA 3D camera.

Acknowledgements

We would like to thank the City of Victoria for helping to coordinate the drone data acquisition and providing access to the drone and LiDAR data, GlobalMedic for helping to design and coordinate the drone data acquisition, InDro Robotics and Global UAV Technologies for acquiring the drone data, Nav Canada for coordinating the drone flights with the harbor control tower and pilots, and Transport Canada for granting approval for the drone operations. We would also like to acknowledge the support of Alberta Innovates and Alberta Advanced Education.

References

Achille, C., Adami, A., Chiarini, S., Cremonesi, S., Fassi, F., Fregonese, L. and Taffurelli, L.: UAV-based photogrammetry and integrated technologies for architectural applications—methodological strategies for the after-quake survey of vertical structures in Mantua (Italy), Sensors (Switzerland), 15(7), 15520–15539, doi:10.3390/s150715520, 2015.

AIR Worldwide: Study of Impact and the Insurance and Economic Cost of a Major Earthquake in British Columbia and Ontario/Quebec, The Insurance Bureau of Canada, AIR Worldwide, Boston, MA, USA, 2013.

Alsadik, B., Gerke, M. and Vosselman, G.: Visibility analysis of point cloud in close range photogrammetry, in: ISPRS Annals of the Photogrammetry, Remote Sensing and Spatial Information Sciences, ISPRS Technical Commission V Symposium, Riva del Garda, Italy, 23-25 June 2014, 9-16, 2014.

American Society for Photogrammetry and Remote Sensing (ASPRS): ASPRS Positional Accuracy Standards for Digital Geospatial Data, Photogramm. Eng. Remote Sens., 81(3), 1–26, doi:10.14358/PERS.81.3.A1-A26, 2015.

Calantropio, A., Chiabrando, F., Sammartano, G., Spanò, A., and Losè, L. T.: UAV Strategies Validation and Remote Sensing Data for Damage Assessment in Post-Disaster Scenarios, in: The International Archives of the Photogrammetry, Remote Sensing and Spatial Information Sciences, Volume XLII-3/W4, 2018 GeoInformation For Disaster Management (Gi4DM), Istanbul, Turkey, 18–21 March 2018, 121-128, 2018.

City of Victoria (CoV): Downtown Core Area Plan, City of Victoria Sustainable Planning and Community Development Department, Victoria, BC, Canada, 2011.

CloudCompare. (2018). CloudCompare (version 2.9.1) [Software]. Available from http://www.cloudcompare.org/

Copernicus Emergency Management Service (Copernicus EMS): How the Copernicus Emergency Management Service supported responses to major earthquakes in Central Italy [online] Available from: http://emergency.copernicus.eu/mapping/ems/how-copernicus-emergency-management-service-supported-responses-major-earthquakes-central-italy, 2017.

Cusicanqui, J., Kerle, N. and Nex, F.: Usability of aerial video footage for 3-D scene reconstruction and structural damage assessment, Nat. Hazards Earth Syst. Sci., 18, 1583–1598, doi:10.5194/nhess-18-1583-2018, 2018.

Dominici, D., Alicandro, M. and Massimi, V.: UAV photogrammetry in the post-earthquake scenario: case studies in L'Aquila, Geomatics, Nat. Hazards Risk, 8(1), 87–103, doi:10.1080/19475705.2016.1176605, 2017.

ESRI. (2018). ArcMap (version 10.5.1) [Software]. Redlands, CA: Environmental Systems Research Institute.

Fernandez Galarreta, J., Kerle, N. and Gerke, M.: UAV-based urban structural damage assessment using object-based image analysis and semantic reasoning, Nat. Hazards Earth Syst. Sci., 15, 1087–1101, doi:10.5194/nhess-15-1087-2015, 2015.

Fonstad, M. A., Dietrich, J. T., Courville, B. C., Jensen, J. L. and Carbonneau, P. E.: Topographic structure from motion: A new development in photogrammetric measurement, Earth Surf. Process. Landforms, 38(4), 421–430, doi:10.1002/esp.3366, 2013.

~~García-Quijano, M. J., Jensen, J. R., Hodgson, M. E., Hadley, B. C., Gladden, J. B. and Lapine, L. A.: Significance of Altitude and Posting Density on Lidar-derived Elevation Accuracy on Hazardous Waste Sites, Photogramm. Eng. Remote Sens., 74(9), 1137–1146, doi:10.14358/PERS.74.9.1137, 2008.~~

Hugenholtz, C. H., Whitehead, K., Brown, O. W., Barchyn, T. E., Moorman, B. J., LeClair, A., Riddell, K. and Hamilton, T.: Geomorphological mapping with a small unmanned aircraft system (sUAS): Feature detection and accuracy assessment of a photogrammetrically-derived digital terrain model, Geomorphology, 194, 16–24, doi:10.1016/j.geomorph.2013.03.023, 2013.

Hugenholtz, C., Brown, O., Walker, J., Barchyn, T., Nesbit, P., Kucharczyk, M. and Myshak, S.: Spatial accuracy of UAV-derived orthoimagery and topography: Comparing photogrammetric models processed with direct geo-referencing and ground control points, Geomatica, 70(1), doi:10.5623/cig2016-102, 2016.

Kakooei, M. and Baleghi, Y.: Fusion of satellite, aircraft, and UAV data for automatic disaster damage assessment, Int. J. Remote Sens., 38(8–10), 2511–2534, doi:10.1080/01431161.2017.1294780, 2017.

Masi, A., Chiauzzi, L., Santarsiero, G., Liuzzi, M. and Tramutoli, V.: Seismic damage recognition based on field survey and remote sensing: general remarks and examples from the 2016 Central Italy earthquake, Nat. Hazards, 86, 193–195, doi:10.1007/s11069-017-2776-8, 2017.

Meyer, D., Hess, M., Lo, E., Wittich, C. E., Hutchinson, T. C. and Kuester, F.: UAV-based post disaster assessment of cultural heritage sites following the 2014 South Napa Earthquake, 2015 Digit. Herit. Int. Congr. Digit. Herit. 2015, 421–424, doi:10.1109/DigitalHeritage.2015.7419539, 2015.

Moya, L., Yamazaki, F., Liu, W., Chiba, T. and Mas, E.: Detection of Collapsed Buildings Due To the 2016 Kumamoto Earthquake From Lidar Data, Nat. Hazards Earth Syst. Sci., 18, 65–78, doi:10.5194/nhess-18-65-2018, 2018.

Pix4D. (2018). Pix4Dmapper (version 4.3.27) [Software]. Lausanne, Switzerland: Pix4D.

Pu, R.: A Special Issue of Geosciences: Mapping and Assessing Natural Disasters Using Geospatial Technologies, Geosciences, 7(4), 4, doi:10.3390/geosciences7010004, 2017.

Rupnik, E., Nex, F., Toschi, I. and Remondino, F.: Aerial multi-camera systems : Accuracy and block triangulation issues, ISPRS J. Photogramm. Remote Sens., 101(60), 233–246, 2015.

senseFly. (2018). eMotion (version 3) [Software]. Cheseaux-sur-Lausanne, Switzerland: senseFly.

United Nations: World Urbanization Prospects: The 2018 Revision [key facts], Population Division, United Nations, New York, New York, USA, 2018.

VC Structural Dynamics Ltd: Executive Summary, Citywide Seismic Vulnerability Assessment of The City of Victoria, The Corporation of the City of Victoria, Victoria, BC, Canada, 2016.

Vetrivel, A., Gerke, M., Kerle, N. and Vosselman, G.: Identification of damage in buildings based on gaps in 3D point clouds from very high resolution oblique airborne images, ISPRS J. Photogramm. Remote Sens., 105, 61–78, doi:10.1016/j.isprsjprs.2015.03.016, 2015.

Vetrivel, A., Gerke, M., Kerle, N., Nex, F. and Vosselman, G.: Disaster damage detection through synergistic use of deep learning and 3D point cloud features derived from very high resolution oblique aerial images, and multiple-kernel-learning, ISPRS J. Photogramm. Remote Sens., 140, 45–59, doi:10.1016/j.isprsjprs.2017.03.001, 2018.

Westoby, M. J., Brasington, J., Glasser, N. F., Hambrey, M. J. and Reynolds, J. M.: “Structure-from-Motion” photogrammetry: A low-cost, effective tool for geoscience applications, Geomorphology, 179, 300–314, doi:10.1016/j.geomorph.2012.08.021, 2012.

Wu, B., Xie, L., Hu, H., Zhu, Q. and Yau, E.: Integration of aerial oblique imagery and terrestrial imagery for optimized 3D modeling in urban areas, ISPRS J. Photogramm. Remote Sens., 139, 119–132, doi:10.1016/j.isprsjprs.2018.03.004, 2018.

Table 1. DSMs generated with different processing settings in Pix4D (v4.3.27), with number of minutes for each step, total time in hours, and resulting RMSE$_z$. The processing was done using a high-performance computer (Intel® Core™ i9-7900X CPU @ 3.30 GHz with 64 GB RAM and NVIDIA GeForce GTX 1080 GPU).

	Processing settings		**Processing time (min)**				
DSM	Image scale	Point density	Initial processing	Point cloud densification	DSM generation	Total processing time (h)	DSM RSME$_z$ (m)
Rapid1	1/8	Low	8.97	9.78	11.15	0.50	0.16
Rapid2	1/4	Low	13.07	13.60	10.80	0.62	0.~~12~~14
Rapid3	1/2	Low	22.15	28.62	13.57	1.07	0.~~10~~11
Rapid4	1	Low	25.73	105.22	28.08	2.65	0.08
Slow	1	Medium	25.83	361.00	101.80	8.14	0.~~07~~08

Table 2. Hypothetical DoDs calculated using different DSM combinations. The LoD for each DoD was calculated using Eq (2).

DoD	**Pre-disaster DSM**	**Post-disaster DSM**	**RMSE$_{z1}$ (m)[a]**	**RMSE$_{z2}$ (m)[b]**	**LoD (m)**
DoD1	RTK/PPK drone (“Slow”)	RTK/PPK drone (“Slow”)	0.~~07[c]~~08[c]	0.~~07[c]~~08[c]	0.~~30~~34
DoD2	LiDAR	RTK/PPK drone (“Slow”)	0.~~07[d]~~04[d]	0.~~07[c]~~08[c]	0.~~30~~27
DoD3	RTK/PPK drone (“Slow”)	RTK/PPK drone (“Rapid1”)	0.~~07[c]~~08[c]	0.16[e]	0.~~52~~54
DoD4	LiDAR	RTK/PPK drone (“Rapid1”)	0.~~07[d]~~04[d]	0.16[e]	0.~~52~~49
DoD5	Non-RTK/PPK drone	Non-RTK/PPK drone	2.14[f]	2.14[f]	9.10
DoD6	LiDAR	Non-RTK/PPK drone	0.~~07[d]~~04[d]	2.14[f]	6.~~44~~43

[a]RMSE$_z$ of the pre-disaster DSM.

[b]RMSE$_z$ of the post-disaster DSM.

[c]RMSE$_z$ of “Slow” DSM, as shown in Table 1.

[d]RMSE$_z$ of the ~~a TIN generated from a bare-earth LiDAR point cloud with an average point spacing of 0.61 m, from García-Quijano et al. (2008).~~LiDAR DSM.

[e]RMSE$_z$ of “Rapid1” DSM, as shown in Table 1.

[f]RMSE$_z$ of a DSM generated using a non-RTK/PPK senseFly eBee (no GCPs), from Hugenholtz et al. (2016).

Figure 1. Geospatial accuracy results for the "slow" DSM: (a) vertical error histogram with statistics and Shapiro-Wilk (S-W) *p*-value, and (b) DSM of difference, calculated by subtracting DSM_{LiDAR} from DSM_{drone}. Blue tints represent elevation overestimations and red tints represent elevation underestimations by DSM_{drone}. Buildings with major contiguous DSM differences are boxed in black. The causes of these contiguous DSM differences are due to changes during the 5 years between LiDAR (2013) and drone (2018) data acquisition, including new construction (1, 2, 4–10, 12, 14–16), structure removal (3, 5, 11), and parking lot excavation (13).

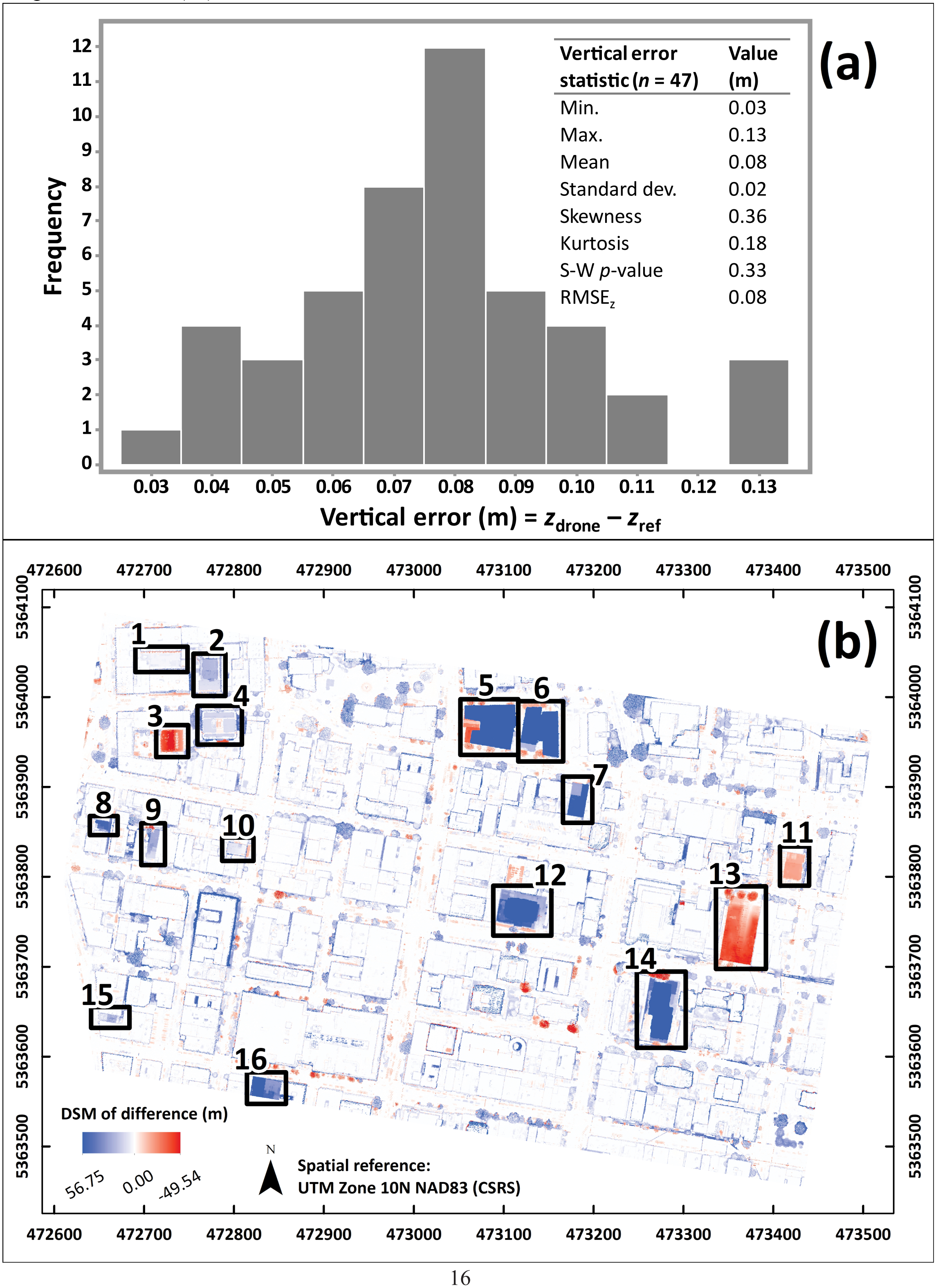

Figure 2. Sample buildings segmented from the dense point cloud (colored by 3D point density), medium-resolution mesh, and high-resolution mesh. Both meshes were generated using identical input imagery and processing settings, except for the mesh resolution setting. Google 3D is shown as a reference for building appearance.

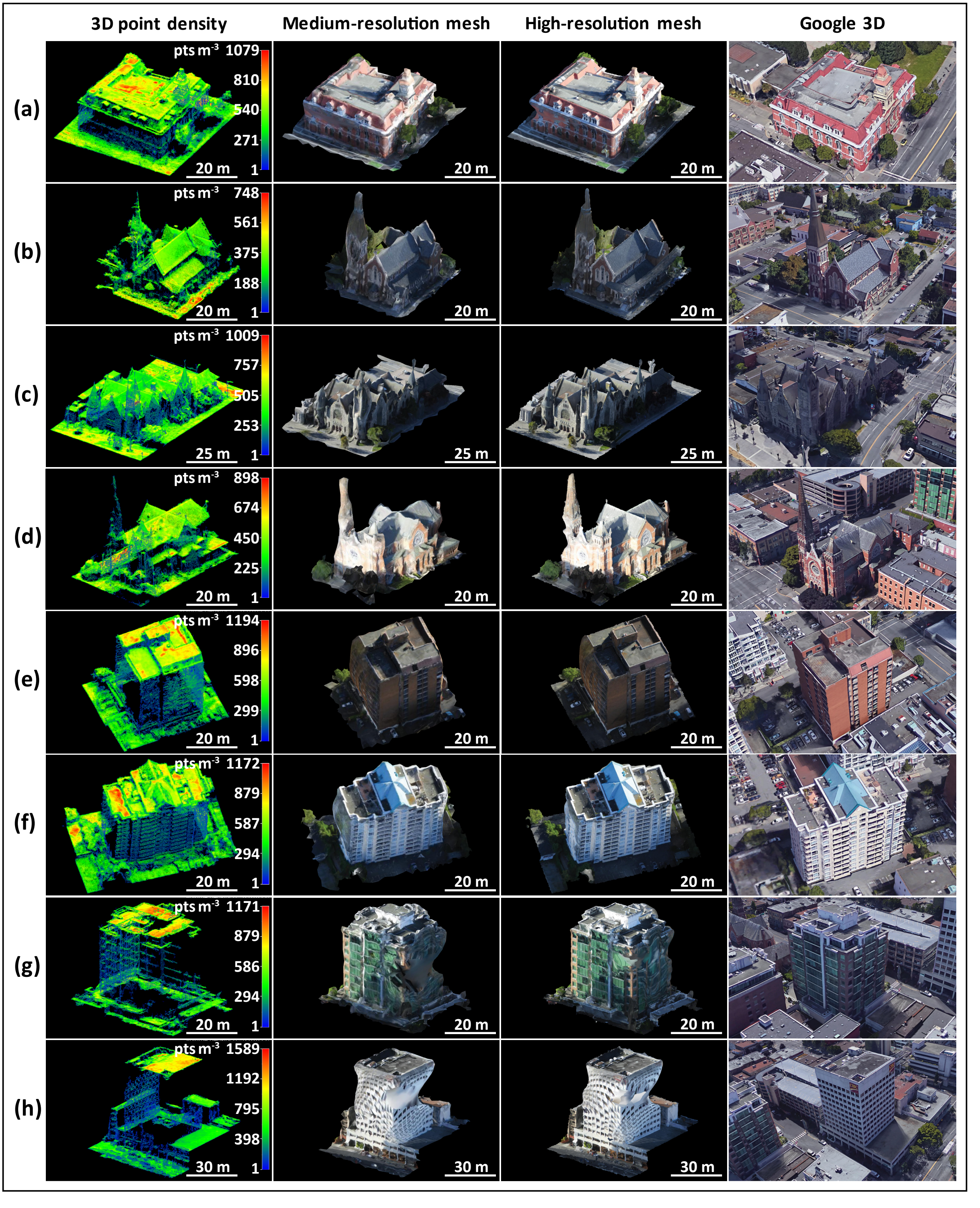

Figure 3. Sample building facades, each represented by a 0.50 m 3D point density raster, and a high-resolution mesh segmentation. Red cells within each raster represent data gaps (0 points per cell).